Supporting Information

A Stable Dysprosium(III) Complex with Terminal Fluoride Ligand Showing High Resolution Luminescence and Slow Magnetic Relaxation

Bo-Kai Ling,[a] Yuan-Qi Zhai,[a] Junbo Han,[b] Tian Han*,[a] and Yan-Zhen Zheng*,[a]

[a] *Frontier Institute of Science and Technology (FIST), Xi'an Jiaotong University Shenzhen Research School, State Key Laboratory of Mechanical Behavior for Materials, MOE Key Laboratory for Nonequilibrium Synthesis of Condensed Matter, Xi'an Key Laboratory of Sustainable Energy and Materials Chemistry, School of Science, Xi'an Jiaotong University, 99 Yanxiang Road, Xi'an, Shaanxi 710054, China*

[b] *Wuhan National High Magnetic Center, Huazhong University of Science and Technology, Wuhan 430074, China*

Corresponding author.
E-mail address: hantian0123@xjtu.edu.cn (T. Han); zheng.yanzhen@xjtu.edu.cn (Y.-Z. Zheng).

Materials and Measurements

All reagents and solvents for the syntheses were purchased from commercial sources and used as received. **$[Dy_2(O_2C^tBu)_6(HO_2C^tBu)_6]$** was prepared as described previously.[1] Magnetic susceptibility measurements were performed on a powder sample fixed with eicosane on a Quantum Design MPMS-XL7 SQUID magnetometer. Diamagnetic corrections were made with Pascal's constants for all the constituent atoms, eicosane and sample holder. Elemental analyses (C, H and N) were performed on a Vario EL III elemental analyzer. XPS experiment was performed on a Thermo Fisher ESCALAB Xi+ analyzer. XRD experiment was performed on a Rigaku Smartlab X-ray diffractometer. Infrared spectra (4000-400cm-1) of all samples were recorded on a Thermo Scientific Nicolet 6700 FT-IR spectrophotometer. Room temperature luminescence spectra were performed on Edinburgh FLS980 Spectrometer. Low temperature luminescence spectra at 4.2 K were measured in Wuhan National High Magnetic Center and the mass of sample was 4 mg.

1. Synthesis

Synthesis of **$[C(NH_2)_3]_4[DyF(piv)_4](piv)_2$ (1)**: $Dy_2(piv)_6(Hpiv)_6$ (760 mg, 0.50 mmol), NH_4F (74 mg, 2 mmol) and guanidine carbonate (242 mg, 2 mmol) were dissolved in 8 mL acetonitrile. After 10 min ultrasonic treatment, the bomb was sealed and heated at 150 ℃ for 72 h. After cooling down to room temperature, colorless single crystals were isolated in 10-15% yield based on Dy. Elemental analyses for $DyFC_{34}H_{78}N_{12}O_{12}$, calculated: C, 39.70, H, 7.61, N, 16.34; found: C, 39.60, H 7.55, N, 16.10.

2. Crystallography

Single-crystal X-ray diffraction data were collected on a Bruker Apex II DUO diffractometer at 150, 293, 400 and 473 K. The structures were solved by direct methods and all non-H atoms were subjected to anisotropic refinement by full-matrix least-squares refinement on F^2 using SHELXTL. Data can be obtained free of charge via www.ccdc.cam.ac.uk/data_request/cif.

Table S1. Crystal data and structure refinement for complex **1**.

Compound	**1**			
Formula	$DyFC_{34}H_{78}N_{12}O_{12}$	$DyFC_{34}H_{78}N_{12}O_{12}$	$DyFC_{34}H_{78}N_{12}O_{12}$	$DyFC_{34}H_{78}N_{12}O_{12}$
Formula weight	1028.58	1028.58	1028.58	1028.58
Temperature / K	150	293	400	473
Crystal system	monoclinic	monoclinic	monoclinic	monoclinic
Space group	$P2_1/c$	$P2_1/c$	$P2_1/c$	$P2_1/c$
a/Å	17.676(9)	17.763(7)	17.739(7)	17.87(7)
b/Å	13.168(7)	13.246(4)	13.289(5)	13.40(5)
c/Å	22.406(12)	22.554(7)	22.613(8)	22.78(10)
α/°	90	90	90	90
β/°	90.934(8)	90.957(2)	91.047(5)	91.02(3)
γ/°	90	90	90	90
V/Å^3	5214(5)	5306(3)	5330(3)	5453(39)
Z	4	4	4	4
ρ_{calc} / g cm^{-3}	1.310	1.288	1.282	1.253
μ/mm^{-1}	1.497	1.471	1.465	1.432
GOF[a]	1.036	1.046	1.001	1.026
R_1, wR_2 [$I > 2\sigma(I)$] [b]	0.0443, 0.1097	0.0419, 0.1151	0.0464, 0.1083	0.0774, 0.2095
R_1, wR_2 (all data)	0.0632, 0.1233	0.0750, 0.1420	0.1008, 0.1348	0.1584, 0.2900
CCDC number	1985213	1985214	1985215	1985216

[a] $GOF = [\Sigma w(F_o^2 - F_c^2)^2/(n_{obc} - n_{param})]^{1/2}$.

[b] $R_1 = ||F_o| - |F_c||/\Sigma|F_o|$, $wR_2 = [\Sigma w(F_o^2 - F_c^2)^2/\Sigma w(Fo^2)^2]^{1/2}$.

3. Photographs of structure

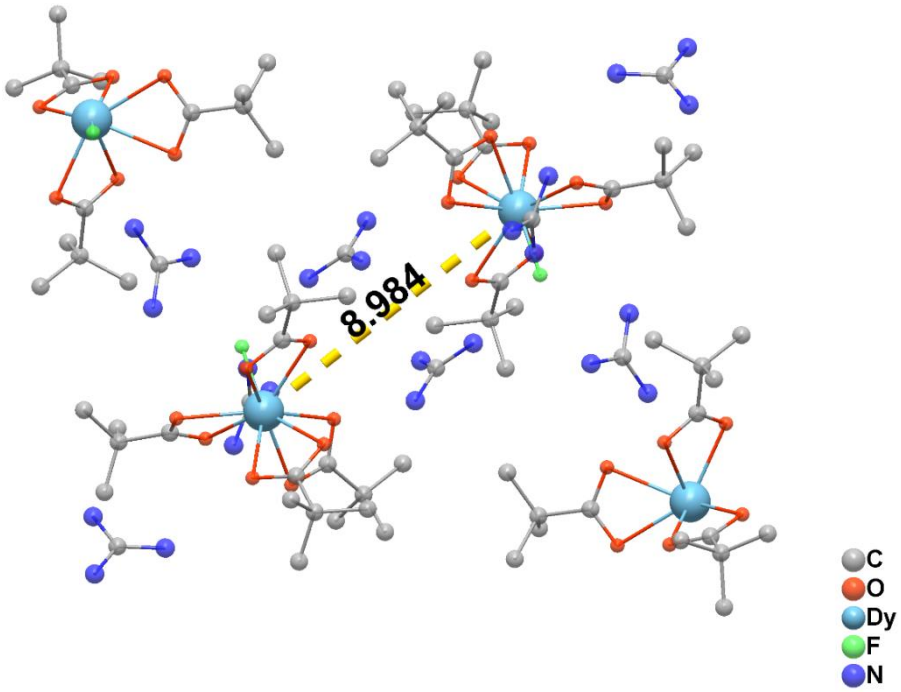

Fig. S1. The shortest distance between Dy ions for complex **1**.

4. Basic characterizations for complex 1

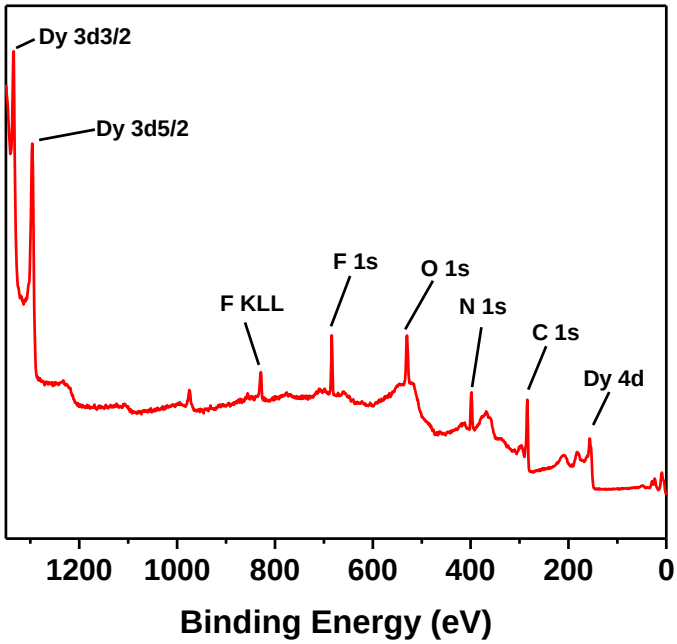

Fig. S2. XPS spectrum for complex **1**. On the surface of washed sample, the detected binding energies of Dy 3d3/2, Dy 3d5/2, Dy 4d, C 1s, N 1s and O 1s locate at 1334, 1296, 157, 284 398 and 531 eV. The obvious F 1s and KLL peaks are observed at 684 and 829 eV, respectively, giving a strong evidence for the terminal F^- ion.

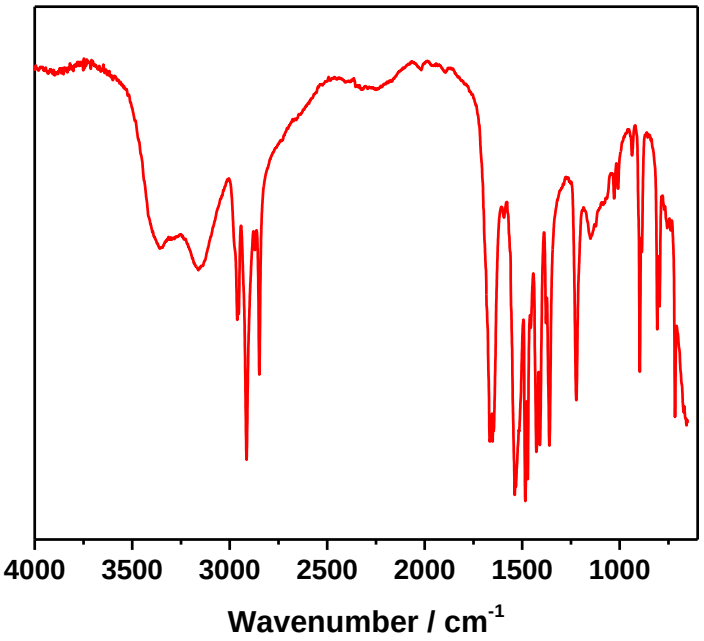

Fig. S3. IR spectrum for complex **1**.

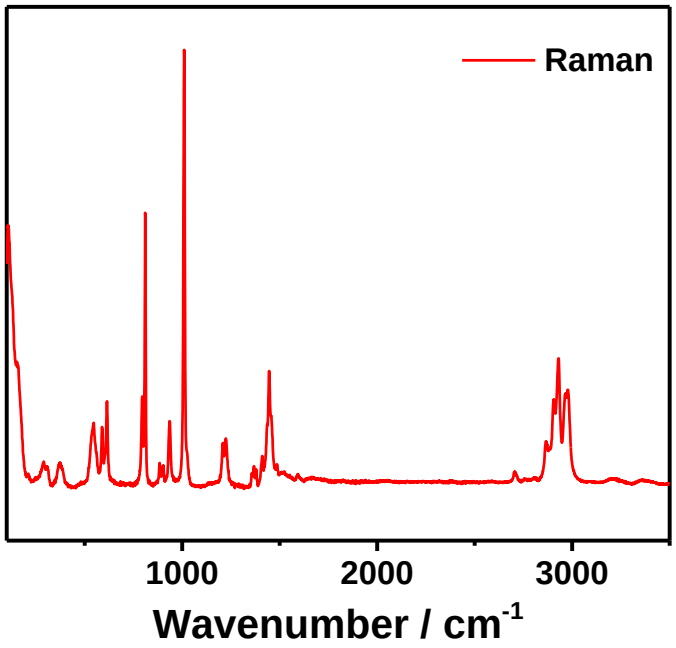

Fig. S4. Raman spectrum for complex **1**.

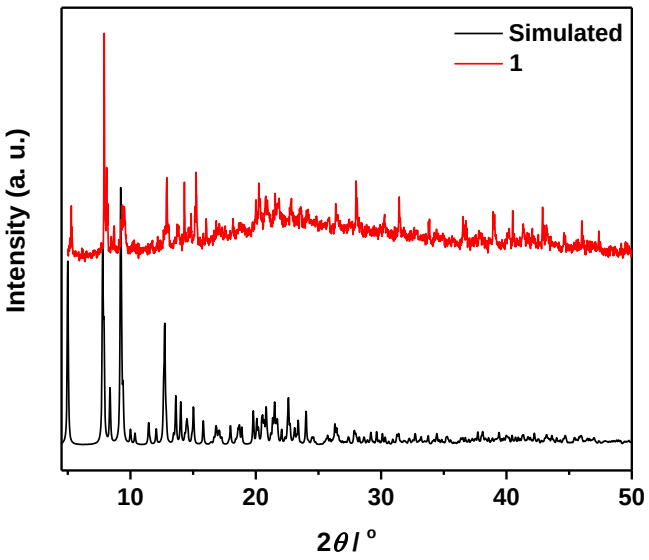

Fig. S5. XRD for complex **1**.

5. Continuous Shape Measurement

Table S2: Continuous Shape Measures (CShM) calculations for complex **1**.

Lable	Shape	Symmetry	
EP-9	Enneagon	D_{9h}	34.660
OPY-9	Octagonal pyramid	C_{8v}	20.965
HBPY-9	Heptagonal bipyramid	D_{7h}	14.345
JTC-9	Johnson triangular cupola J3	C_{3v}	14.800
JCCU-9	Capped cube J8	C_{4v}	7.002
CCU-9	Spherical-relaxed capped cube	C_{4v}	5.762
JCSAPR-9	Capped square antiprism J10	C_{4v}	3.919
CSAPR-9	Spherical capped square antiprism	C_{4v}	3.097
JTCTPR-9	Tricapped trigonal prism J51	D_{3h}	5.172
TCTPR-9	Spherical tricapped trigonal prism	D_{3h}	3.978
JTDIC-9	Tridiminished icosahedron J63	C_{3v}	11.212
HH-9	Hula-hoop	C_{2v}	8.548
MFF-9	Muffin	C_s	2.651

6. The environment of H-bond in complex 1

Table S3. Distances and angles of H-A, D-A[a] distances in complex 1

H-bond for F	**Distance for H-A**	**Distance of D-A**	**Angle of H-bond**
F1-H1B- N1	2.010(2)	2.857(5)	161.32(27)
F1-H2A- N2	2.239(2)	2.927(5)	134.95(26)
F1-H4E- N4	1.995(2)	2.813(4)	153.94(25)
H-bond for O[b]			
O1-H10D-N10	2.001(3)	2.848(5)	161.06(29)
O2-H5D-N5	2.000(3)	2.833(6)	156.96(28)
O3-H11A-N11	2.113(3)	2.983(6)	169.34(31)
O5-H1A-N1	2.164(3)	2.974(6)	152.81(32)
O6-H9D-N9	1.996(3)	2.860(5)	167.08(25)
O7-H7A-N7	2.155(3)	2.996(5)	159.72(25)
O8-H6B-N6	2.084(3)	2.949(5)	167.91(25)
H-bond for O[c]			
O9-H9E-N9	2.020(5)	2.802(6)	147.46(29)
O9-H10E-N10	1.987(5)	2.843(7)	163.97(34)
O10-H7B-N7	2.225(4)	2.987(5)	144.79(26)
O10-H8E-N8	2.057(4)	2.861(6)	151.46(34)
O11-H2B-N2	2.018(5)	2.805(7)	148.33(29)
O11-H3E-N3	2.095(6)	2.860(8)	144.82(37)
O12-H5E-N5	2.013(4)	2.852(6)	158.93(28)
O12-H12B-N12	1.989(4)	2.799(6)	152.66(28)

a. D and A means donor and acceptor; b. Oxygen atoms are in coordinate ligands; c. Oxygen atoms are in free ligands. The data in this table is corresponding to the CIF file of complex **1** at 150 K.

Table S4. Eighteen H-bonds in complex **1**

Carbon[a]	Donor[b]	Acceptor[c]
C31	N10	O1, O9
	N11	O3
	N12	O12
C32	N7	O7, O10
	N8	O10
	N9	O9, O6
C33	N1	F1, O5
	N2	O11, F1
	N3	O11
C34	N4	F1
	N5	O2, O12
	N6	O8

a. the label of carbon in guanidine cations; b. the labels of H-bond donors; c. the labels of H-bond acceptors.

O1-O8 are the oxygen atoms in coordinated pivalate ligands and O9-O12 are the oxygen atoms in free pivalate anions.

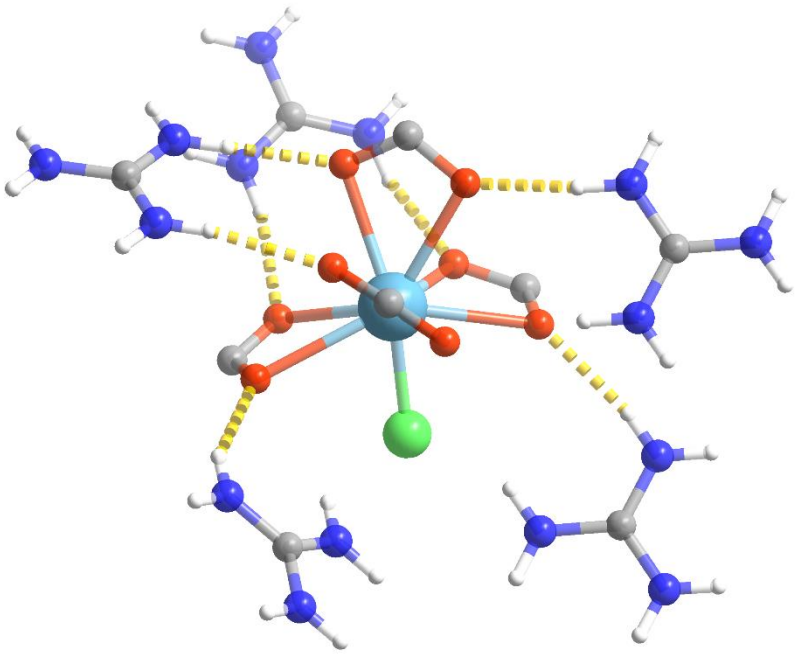

Fig. S6. H-bonds between coordinated pivalate ligands and guanidine cations. The H-bond are highlighted with gold colour and tertiary butyl groups in coordinated pivalate ligands are omitted for clarity.

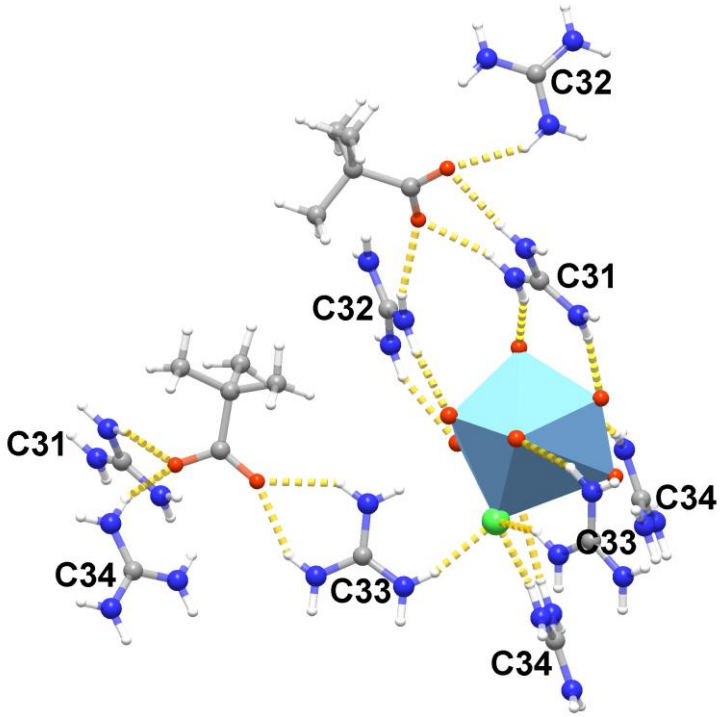

Fig. S7. Eighteen H-bonds (one H-bond is behind the polyhedron) formed by guanidine cations, free pivalate anions and $[DyF(piv)_4]^{2-}$ anion. Labels for carbon atoms in guanidine cations are corresponding to Fig. 2c and Tables S3 and S4. The H-bond are highlighted with gold colour and tertiary butyl groups in coordinated pivalate ligands are omitted for clarity.

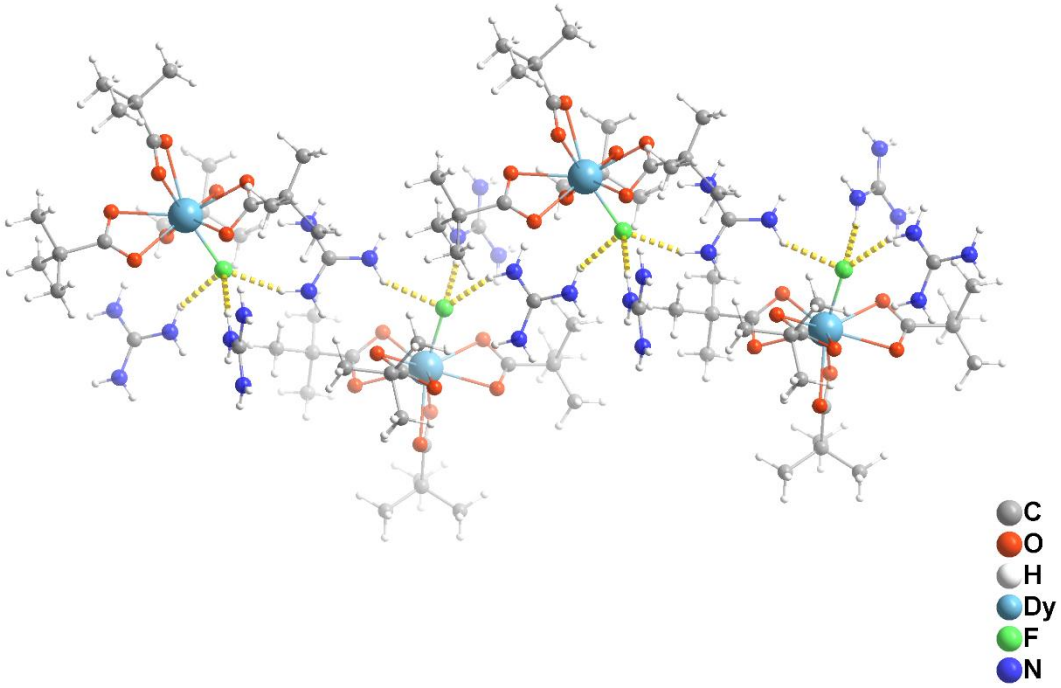

Fig. S8. The H-bond chain formed by fluoride ions and guanidine cations in complex **1**.

7. Coordination bond lengths under different temperatures

Table S5. Coordination bond lengths under different temperatures.

Bond[a]	150 K	293 K	400 K	473 K
Dy-F	2.194(2)	2.204(2)	2.194(3)	2.205(9)
Dy-O1	2.474(3)	2.476(3)	2.468(4)	2.480(12)
Dy-O2	2.444(3)	2.446(3)	2.449(4)	2.463(10)
Dy-O3	2.424(3)	2.436(3)	2.438(4)	2.467(12)
Dy-O4	2.403(3)	2.411(3)	2.403(4)	2.418(10)
Dy-O5	2.557(3)	2.563(3)	2.563(4)	2.587(12)
Dy-O6	2.426(3)	2.427(3)	2.426(4)	2.451(12)
Dy-O7	2.386(3)	2.392(3)	2.406(4)	2.416(9)
Dy-O8	2.494(3)	2.506(3)	2.505(3)	2.512(9)

[a] The labels of atoms are according to the structure at 150 K.

8. Magnetic properties

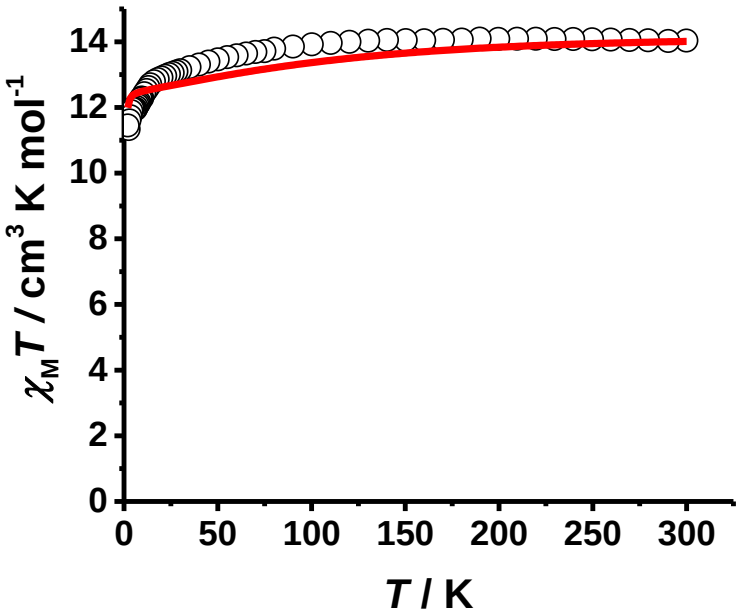

Fig. S9. $\chi_M T$ vs. T for complex **1** in a field of 1000 Oe from 300 to 2 K. The red line shows the simulated plot from *ab initio* calculations.

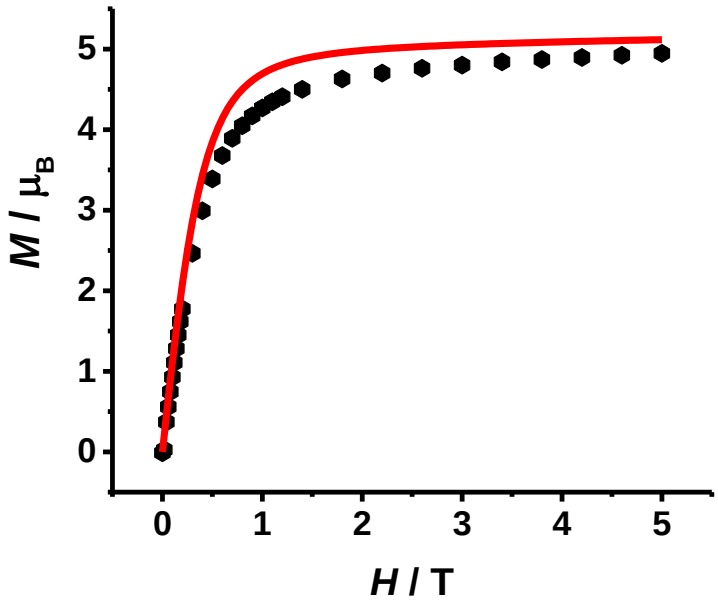

Fig. S10. The field dependence of the magnetization for complex **1** at 2 K. The red line shows the simulated plot from *ab initio* calculations.

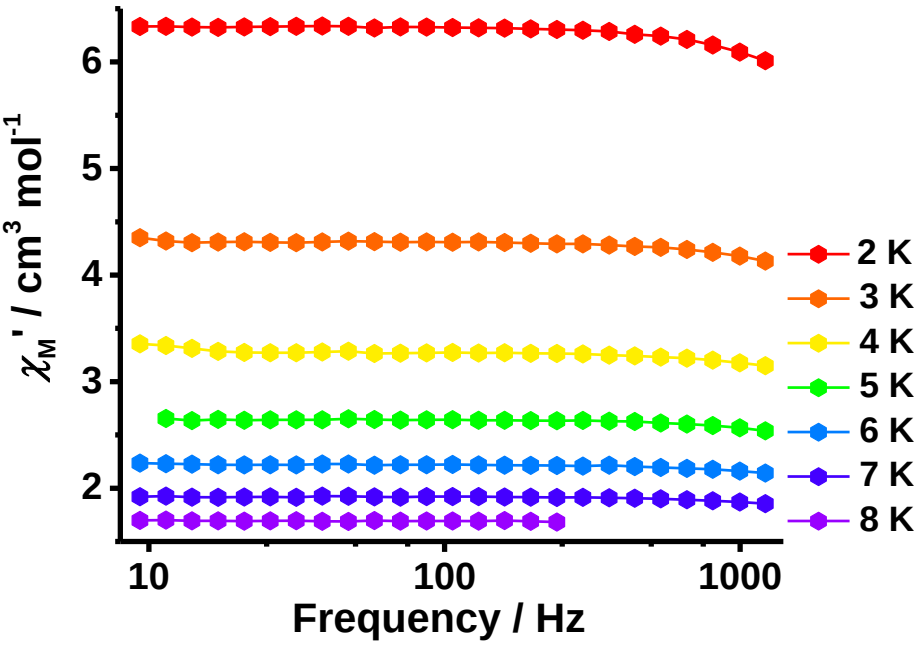

Fig. S11. Frequency dependence of the in-phase susceptibility (χ') in zero dc field at temperatures from 2 to 8 K.

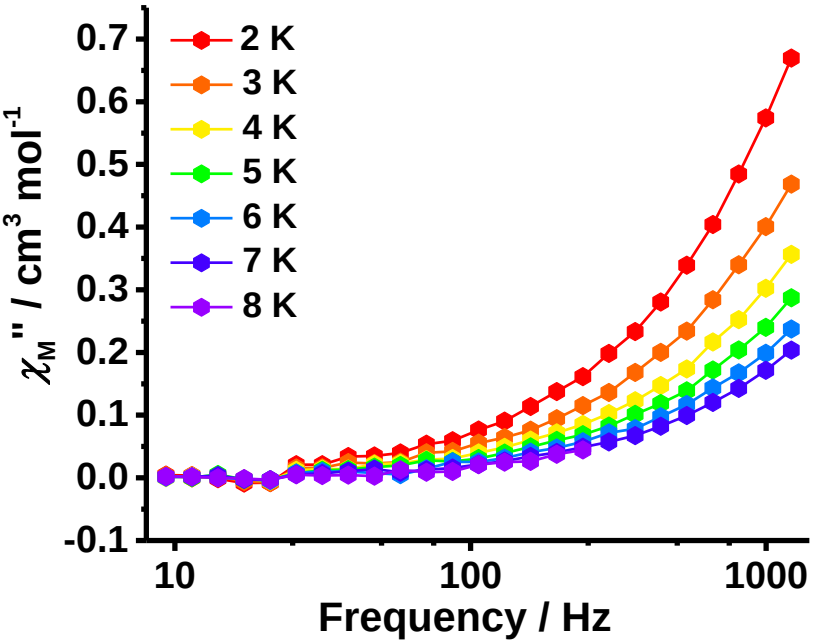

Fig. S12. Frequency dependence of the out-of-phase susceptibility (χ'') in zero dc field at temperatures from 2 to 8 K.

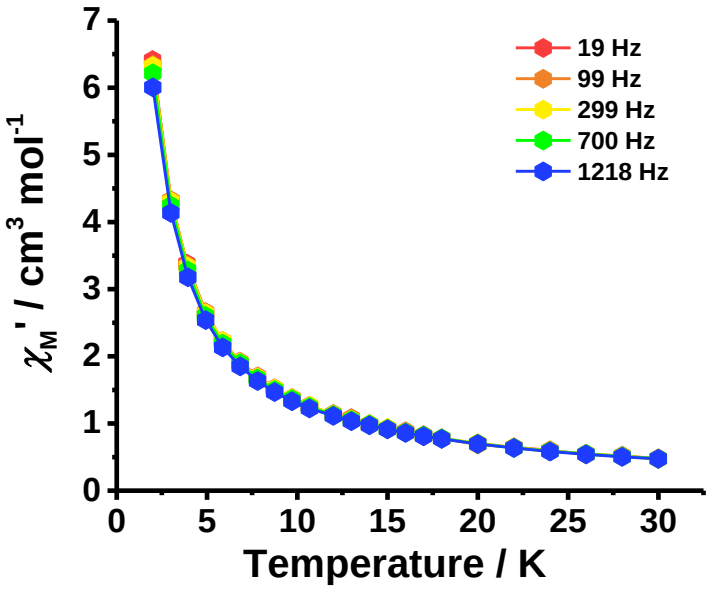

Fig. S13. Temperature dependence of the in-phase susceptibility (χ') in zero dc field with ac frequencies of 19–1218 Hz.

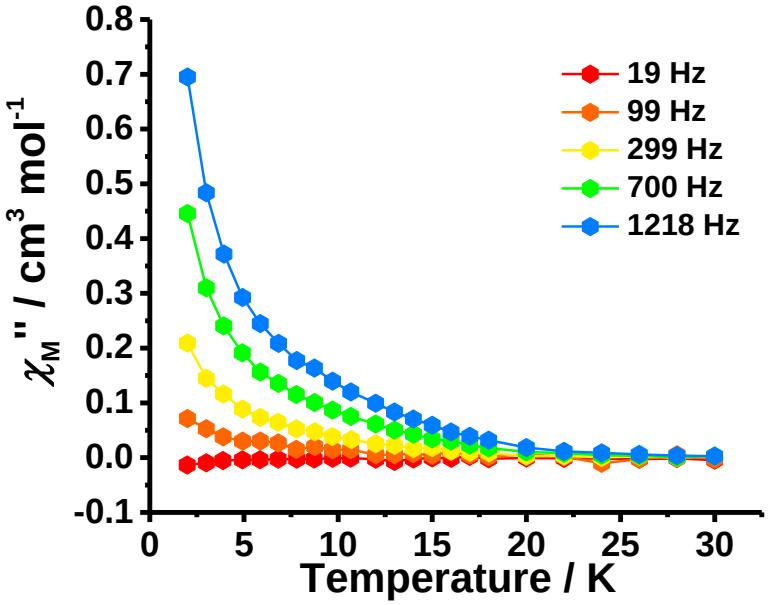

Fig. S14. Temperature dependence of the out-of-phase susceptibility (χ'') in zero dc field with ac frequencies of 19–1218 Hz.

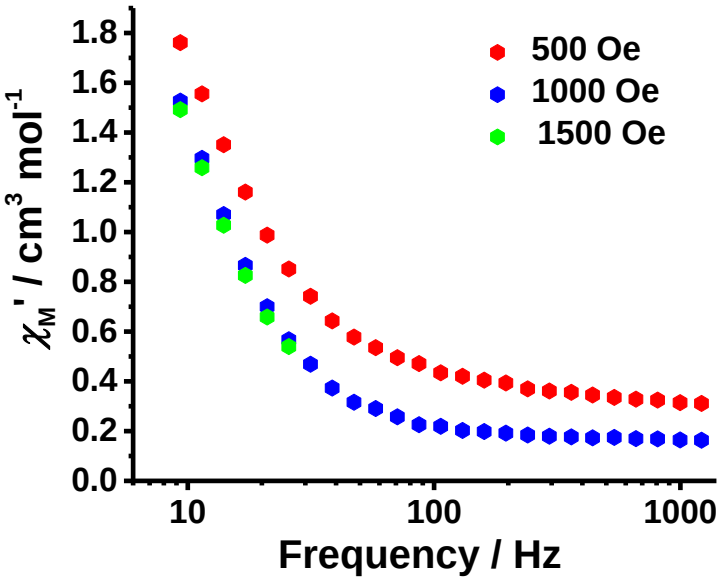

Fig. S15. Frequency dependence of the in-phase susceptibility (χ') for complex **1** under different dc fields at 5 K.

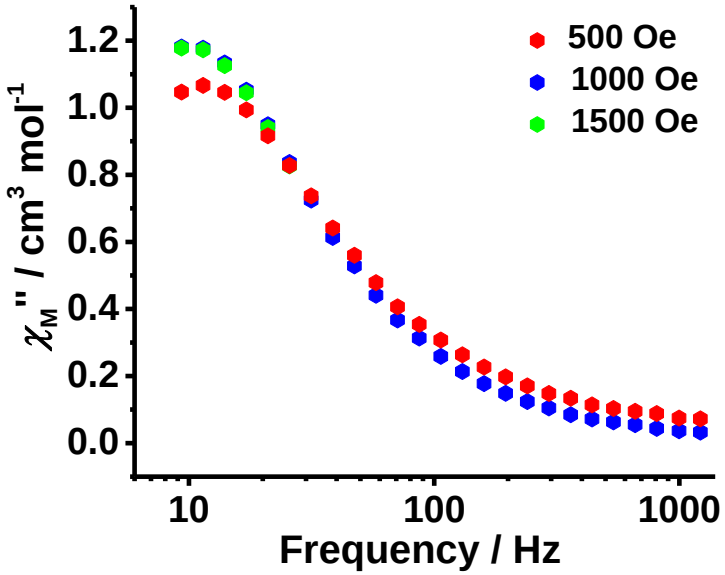

Fig. S16. Frequency dependence of the out-of-phase susceptibility (χ'') for complex **1** under different dc fields at 5 K.

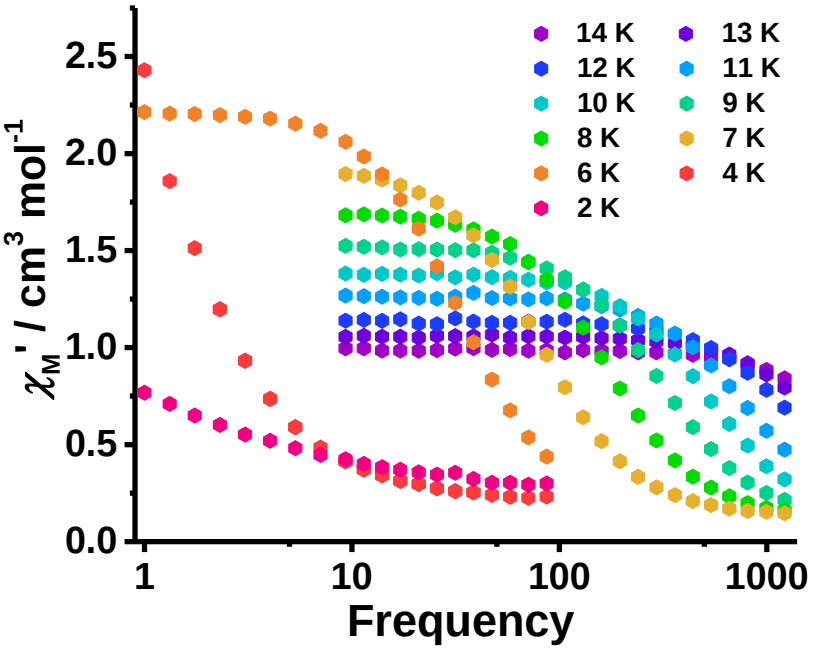

Fig. S17. Frequency dependence of the in-phase susceptibility (χ') in 1000 Oe dc field at temperatures from 2 to 14 K.

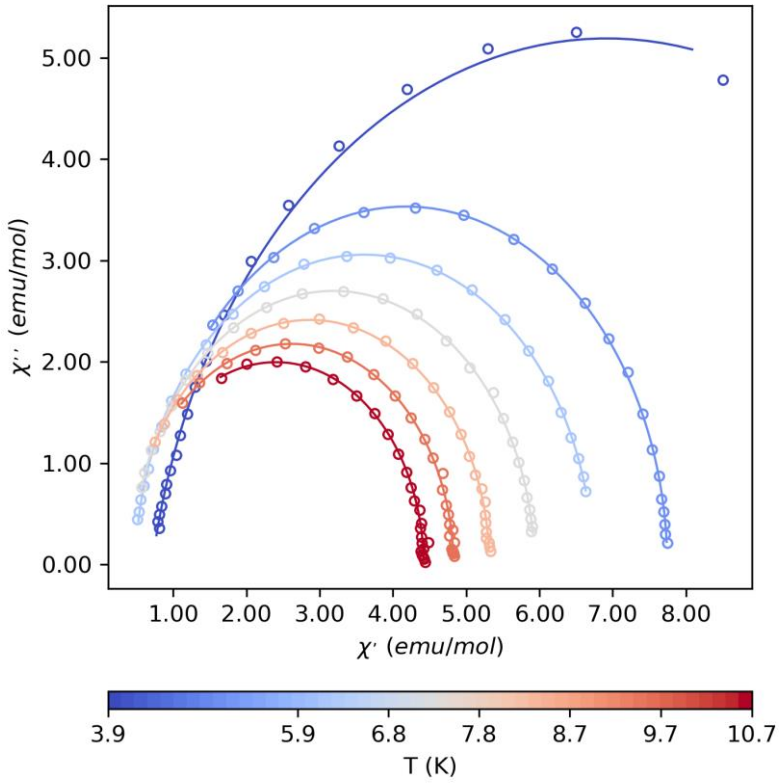

Fig. S18. Cole-Cole plots using the frequency-dependence ac susceptibility data under 1000 Oe dc field for complex **1** from 4 K to 11 K. The solid lines are the best fits.

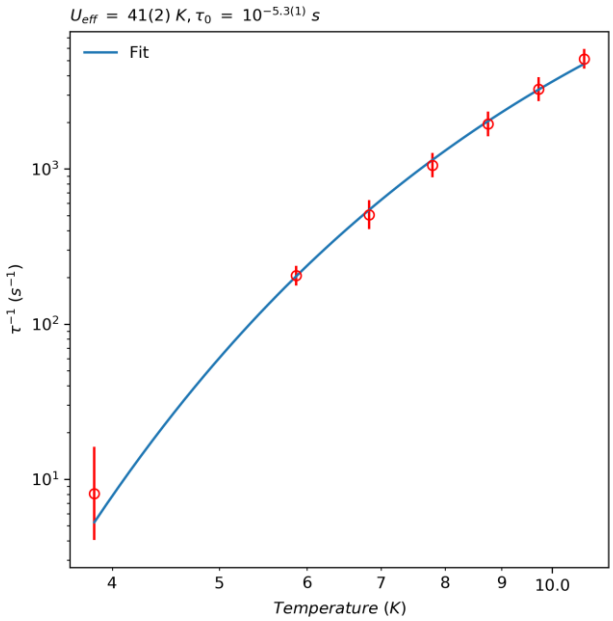

Fig. S19. log–log plot of relaxation time, τ^{-1} vs. T for **1** under 1000 Oe dc field. The solid blue line is the Orbach fit. Due to the small mismatched energy barrier and relatively large prefactor τ_0, the Orbach fit is inappropriate for **1**.

Table S6. Parameters obtained from the fitting of the relaxation times for complex **1**.

T	χ_s	χ_t	τ	α
10.71	0.10981	1.26283	1.95E-04	0.00654
9.70	0.11632	1.37911	3.06E-04	0.00928
8.74	0.11831	1.51968	5.14E-04	0.00998
7.80	0.12726	1.6943	9.47E-04	0.00975
6.80	0.13853	1.92419	0.00197	0.01363
5.86	0.17349	2.21321	0.00487	0.00652
3.77	0.23654	3.52602	0.11454	0.06637

9. Electronic Structure Calculations

Ab initio calculations at SA-CASSCF/RASSI level were performed on program MOLCAS 8.0[2] and the structure was originally taken from the X-Ray structure. The basis sets were chosen from the ANO-RCC library[3] as have been used in many works[4, 5]. The Dy atom was treated with VTZP quality, then the related B, C and O atoms with VDZP quality and others with VDZ quality. The state-averaged CASSCF orbitals of the sextets, quartets and doublets were optimized with 21, 224 and 490 states, respectively, with the RASSCF module. 21, 128 and 130 sextets, quartets and doublets chosen to construct and diagonalizable in spin-orbit (SO) coupling Hamiltonian with the RASSI[6] module. These computed SO states were written into the SINGLE_ANISO[7] program to compute the g-tensors, crystal field parameters and magnetic energy levels for the doublets of the ground $J = 15/2$ multiple of the $^6H_{15/2}$ term for Dy(III). The two electron integrals were Cholesky decomposed with a threshold of 1×10^{-8} to account for the accuracy[8].

Table S7. SA-CASSCF/RASSI calculated electronic states for complex **1**.

Energy (cm^{-1})	Energy (K)	g_x	g_y	g_z	g_z Angle (°)	Wavefunction
0	0	0.007	0.009	19.81	--	96.2%|±15/2>
224	323	0.15	0.15	16.78	3.3	91.3%|±13/2>
339	487	2.32	3.23	13.27	35	65%|±11/2> + 10%|±7/2>
389	559	2.39	4.93	11.26	53	14%|±11/2> + 36%|±9/2> + 15%|±7/2> + 17%|±5/2>
416	598	0.77	3.45	11.69	76	13%|±9/2> + 19%|±5/2> + 30%|±3/2>
443	637	1.80	2.38	13.05	83	14%|±7/2> + 32%|±1/2> + 11%|∓3/2> + 14%|∓7/2>
535	769	0.29	0.93	14.77	86	14%|±7/2> + 15%|±5/2> + 19%|∓1/2> + 14%|∓3/2>
584	840	0.24	1.46	16.87	79	19%|±7/2> + 12%|±3/2> + 18%|±1/2> + 14%|∓3/2> + 20%|∓5/2>

Table S8. *Ab initio* calculated crystal field parameters for complex **1**.

Crystal Field Parameter	Value / cm^{-1}
B_2^{-2}	-0.11064319497114E+00
B_2^{-1}	-0.34588494860981E+00
B_2^0	-0.26524417566797E+01
B_2^1	-0.15498216650057E+00
B_2^2	0.70010505470629E+00
B_4^{-4}	0.14369008080381E-02
B_4^{-3}	-0.20160894320650E-01
B_4^{-2}	0.28457750096773E-02
B_4^{-1}	0.22152129624600E-01
B_4^0	-0.45791730962602E-02
B_4^1	0.11973217441484E-01
B_4^2	-0.26000242420497E-02
B_4^3	-0.15400061016187E-01
B_4^4	-0.76734921211216E-02
B_6^{-6}	0.16199900028512E-04
B_6^{-5}	0.68327344471705E-03
B_6^{-4}	0.35137855965554E-04
B_6^{-3}	0.46861704646308E-03
B_6^{-2}	0.90439594602051E-05
B_6^{-1}	-0.32107248743131E-04
B_6^0	-0.26204659237434E-05
B_6^1	-0.70652835784535E-04
B_6^2	-0.10179167024596E-03
B_6^3	0.14558833297454E-03
B_6^4	-0.63536869356655E-05
B_6^5	-0.63175095044905E-03
B_6^6	-0.24388023436124E-03

Table S9. Average transition magnetic moment elements between the states of complex **1**, given in μ_B^2.

	$\|+\frac{15}{2}\rangle$	$\|-\frac{15}{2}\rangle$	$\|+\frac{13}{2}\rangle$	$\|-\frac{13}{2}\rangle$	$\|+\frac{11}{2}\rangle$	$\|-\frac{11}{2}\rangle$	|+a>	|-a>	|+b>	|-b>	|+c>	|-c>	|+d>	|-d>	|+e>	|-e>
$\|+\frac{15}{2}\rangle$	--	1.6E-05	2.7E-03	4.5E+00	1.0E-02	4.7E-02	5.3E-02	1.5E-02	3.8E-02	7.1E-03	1.6E-02	2.3E-02	2.1E-02	2.8E-03	1.2E-02	2.5E-03
$\|-\frac{15}{2}\rangle$	1.6E-05	--	4.5E+00	2.7E-03	4.7E-02	1.0E-02	1.5E-02	5.3E-02	7.1E-03	3.8E-02	2.3E-02	1.6E-02	2.8E-03	2.1E-02	2.5E-03	1.2E-02
$\|+\frac{13}{2}\rangle$	2.7E-03	4.5E+00	--	5.8E-02	6.3E+00	4.8E-01	8.0E-02	1.3E+00	5.5E-02	4.9E-01	1.2E-01	1.0E-01	1.4E-01	9.1E-02	9.6E-02	1.1E-02
$\|-\frac{13}{2}\rangle$	4.5E+00	2.7E-03	5.8E-02	--	4.8E-01	6.3E+00	1.3E+00	8.0E-02	4.9E-01	5.5E-02	1.0E-01	1.2E-01	9.1E-02	1.4E-01	1.1E-02	9.6E-02
$\|+\frac{11}{2}\rangle$	1.0E-02	4.7E-02	6.3E+00	4.8E-01	--	7.6E+00	2.5E+00	6.8E+00	1.9E+00	9.0E-01	5.9E-01	1.3E+00	3.4E-01	2.1E-01	3.4E-02	1.2E-01
$\|-\frac{11}{2}\rangle$	4.7E-02	1.0E-02	4.8E-01	6.3E+00	7.6E+00	--	6.8E+00	2.5E+00	9.0E-01	1.9E+00	1.3E+00	5.9E-01	2.1E-01	3.4E-01	1.2E-01	3.4E-02
|+a>	5.3E-02	1.5E-02	8.0E-02	1.3E+00	2.5E+00	6.8E+00	--	3.6E+00	6.6E+00	1.4E+00	1.1E+00	1.9E+00	1.2E+00	1.0E+00	1.3E-01	1.5E-01
|-a>	1.5E-02	5.3E-02	1.3E+00	8.0E-02	6.8E+00	2.5E+00	3.6E+00	--	1.4E+00	6.6E+00	1.9E+00	1.1E+00	1.0E+00	1.2E+00	1.5E-01	1.3E-01
|+b>	3.8E-02	7.1E-03	5.5E-02	4.9E-01	1.9E+00	9.0E-01	6.6E+00	1.4E+00	--	7.5E+00	1.0E+01	1.3E+00	5.7E-01	1.1E+00	4.3E-01	3.6E-01
|-b>	7.1E-03	3.8E-02	4.9E-01	5.5E-02	9.0E-01	1.9E+00	1.4E+00	6.6E+00	7.5E+00	--	1.3E+00	1.0E+01	1.1E+00	5.7E-01	3.6E-01	4.3E-01
|+c>	1.6E-02	2.3E-02	1.2E-01	1.0E-01	5.9E-01	1.3E+00	1.1E+00	1.9E+00	1.0E+01	1.3E+00	--	1.1E+01	3.4E+00	1.2E+00	1.0E+00	7.8E-01
|-c>	2.3E-02	1.6E-02	1.0E-01	1.2E-01	1.3E+00	5.9E-01	1.9E+00	1.1E+00	1.3E+00	1.0E+01	1.1E+01	--	1.2E+00	3.4E+00	7.8E-01	1.0E+00
|+d>	2.1E-02	2.8E-03	1.4E-01	9.1E-02	3.4E-01	2.1E-01	1.2E+00	1.0E+00	5.7E-01	1.1E+00	3.4E+00	1.2E+00	--	1.7E+01	6.2E+00	4.1E+00
|-d>	2.8E-03	2.1E-02	9.1E-02	1.4E-01	2.1E-01	3.4E-01	1.0E+00	1.2E+00	1.1E+00	5.7E-01	1.2E+00	3.4E+00	1.7E+01	--	4.1E+00	6.2E+00
|+e>	1.2E-02	2.5E-03	9.6E-02	1.1E-02	3.4E-02	1.2E-01	1.3E-01	1.5E-01	4.3E-01	3.6E-01	1.0E+00	7.8E-01	6.2E+00	4.1E+00	--	2.4E+01
|-e>	2.5E-03	1.2E-02	1.1E-02	9.6E-02	1.2E-01	3.4E-02	1.5E-01	1.3E-01	3.6E-01	4.3E-01	7.8E-01	1.0E+00	4.1E+00	6.2E+00	2.4E+01	--

10. Luminescence.

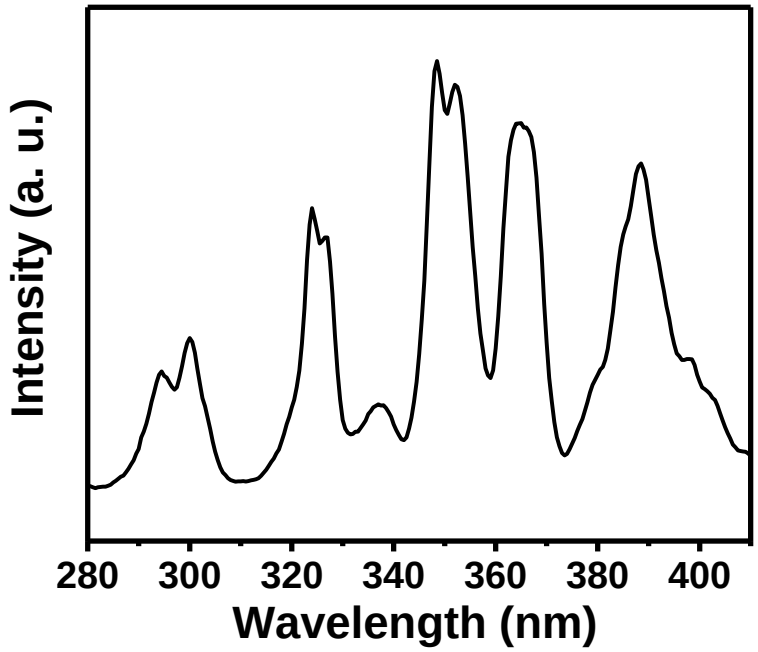

Fig. S20. Excitation spectrum for complex **1** by monitoring 570 nm emission.

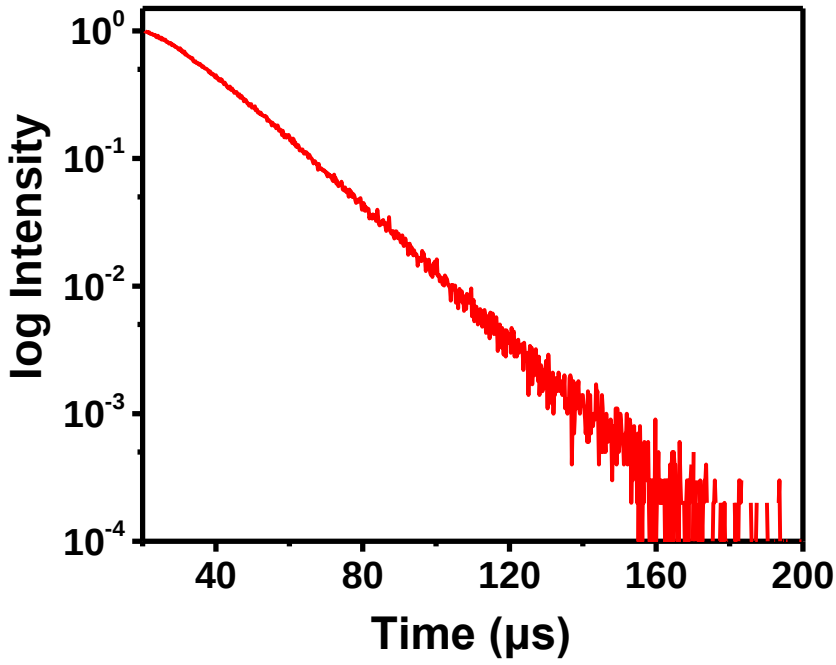

Fig. S21. Decay curve for complex **1** (λ_{ex} = 365 nm and λ_{em} = 480 nm) and the lifetime is 13 μs.

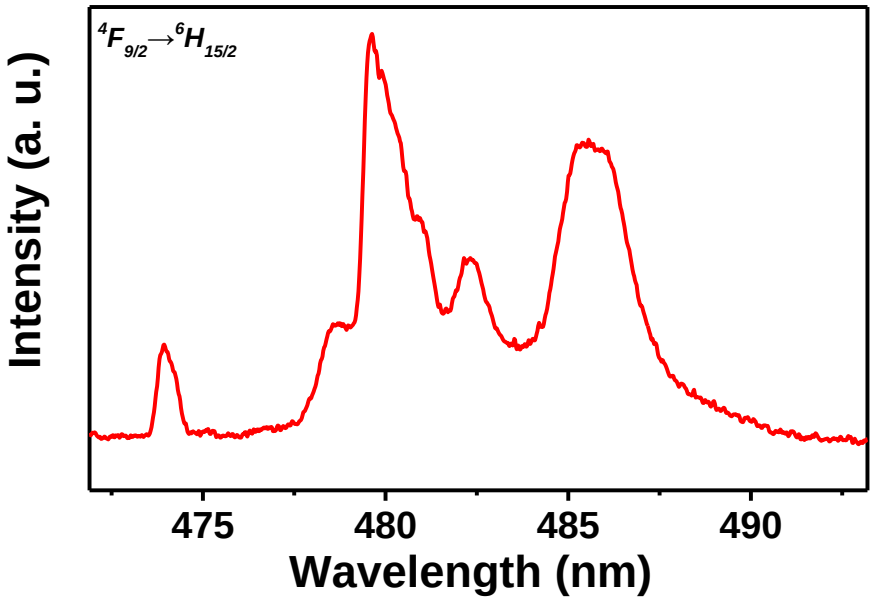

Fig. S22. Fine-spectrum of complex **1** corresponding to $^4F_{9/2}\rightarrow{}^6H_{15/2}$ transition at 4.2 K.

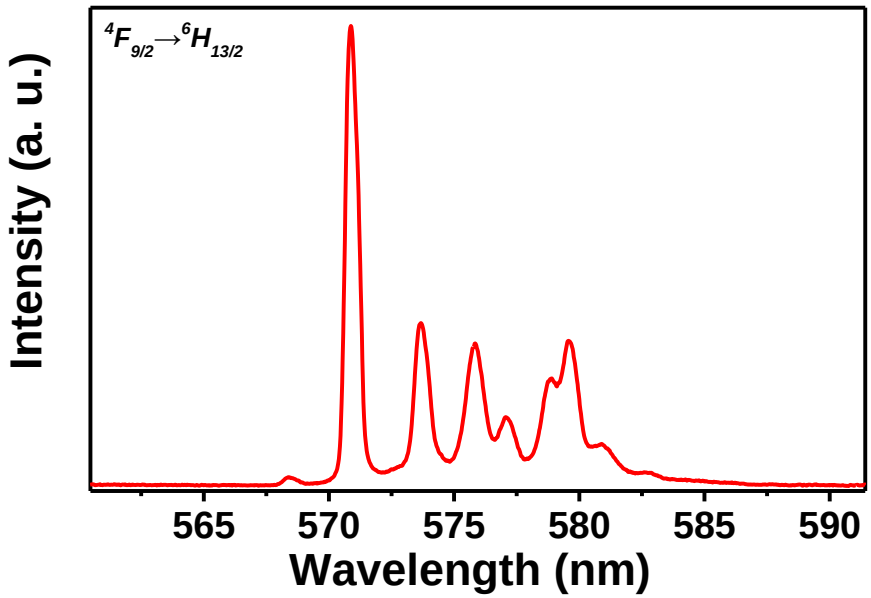

Fig. S23. Fine-spectrum of complex **1** corresponding to $^4F_{9/2}\rightarrow{}^6H_{13/2}$ transition at 4.2 K. The $^4F_{9/2}\rightarrow{}^6H_{13/2}$ transition involves 9 peaks, which is higher than the maximum m_J states expected for $^6H_{13/2}$ multiple (7 components). This can be attributed to vibronic excitations.[9]

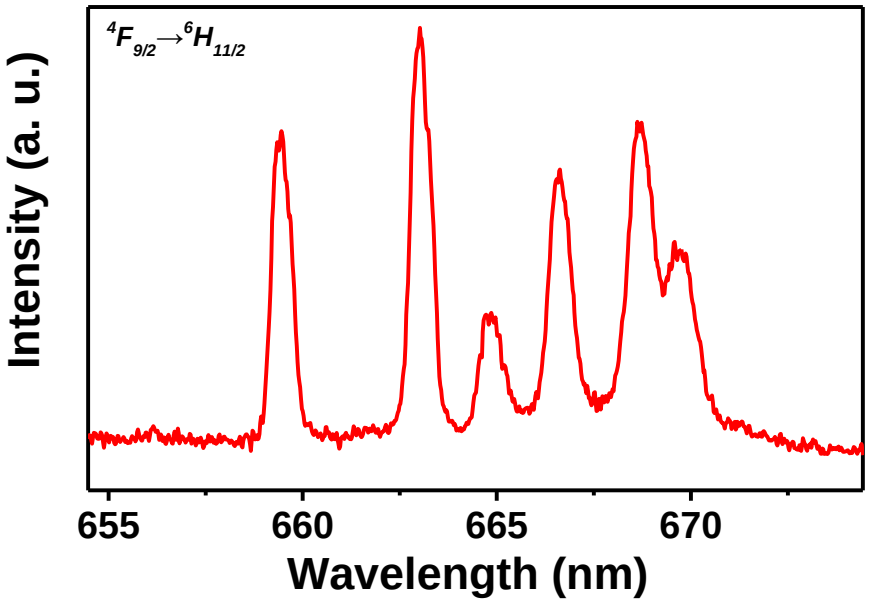

Fig. S24. Fine-spectrum of complex **1** corresponding to $^4F_{9/2}\rightarrow{}^6H_{11/2}$ transition at 4.2 K.

Table S10. Fit parameters corresponding to the ground state splitting of complex **1**

n	Peak (nm)	Width (nm)	E_n-E_1 (cm^{-1})	E_n-E_1 (K)	Height (a.u.)
1	474.0	0.54	0	0	35.9
2	478.5	0.88	197.2	238.8	37.1
3	479.6	0.53	247.0	355.5	75.3
4	480.3	1.73	275.1	396.0	109.6
5	482.4	1.45	365.7	526.4	63.2
6	483.6	0.71	417.9	601.5	17.9
7	4853	2.23	503.2	724.3	104.1
8	487.6	4.20	589.3	848.2	21.1

11. Selected angles for complex 1.

Table S11. Selected angles [deg] for complex **1** at 150 K

F1—Dy1—O1	155.47(10)	F1—Dy1—O2	144.60(9)
F1—Dy1—O3	123.55(11)	F1—Dy1—O4	90.16(10)
F1—Dy1—O5	72.58(10)	F1—Dy1—O6	79.61(10)
F1—Dy1—O7	88.74(11)	F1—Dy1—O8	72.86(10)
O1—Dy1—O5	99.54(10)	O4—Dy1—O6	145.79(10)
O1—Dy1—O8	113.48(10)	O4—Dy1—O8	82.76(11)
O2—Dy1—O5	140.08(10)	O6—Dy1—O5	51.86(11)
O2—Dy1—O1	52.74(10)	O6—Dy1—O2	128.19(10)
O2—Dy1—O8	72.93(11)	O6—Dy1—O1	77.50(10)
O3—Dy1—O2	74.58(11)	O6—Dy1—O8	123.83(11)
O3—Dy1—O1	71.68(11)	O7—Dy1—O5	128.91(11)
O3—Dy1—O6	105.43(10)	O7—Dy1—O2	78.07(11)
O3—Dy1—O8	130.64(10)	O7—Dy1—O4	134.20(11)
O3—Dy1—O5	68.90(11)	O7—Dy1—O3	147.71(12)
O4—Dy1—O5	93.94(11)	O7—Dy1—O1	78.22(11)
O4—Dy1—O2	76.80(11)	O7—Dy1—O6	78.58(11)
O4—Dy1—O3	54.11(10)	O7—Dy1—O8	53.36(10)
O4—Dy1—O1	113.84(11)	O8—Dy1—O5	145.26(11)

12. Reference

1. Y. Z. Zheng, M. Evangelisti and R. E. Winpenny, *Angew. Chem. Int. Ed.*, 2011, **50**, 3692-3695
2. F. Aquilante, J. Autschbach, R. K. Carlson, L. F. Chibotaru, M. G. Delcey, L. De Vico, I. Fdez. Galván, N. Ferré, L. M. Frutos, L. Gagliardi, M. Garavelli, A. Giussani, C. E. Hoyer, G. Li Manni, H. Lischka, D. Ma, P. Å. Malmqvist, T. Müller, A. Nenov, M. Olivucci, T. B. Pedersen, D. Peng, F. Plasser, B. Pritchard, M. Reiher, I. Rivalta, I. Schapiro, J. Segarra-Martí, M. Stenrup, D. G. Truhlar, L. Ungur, A. Valentini, S. Vancoillie, V. Veryazov, V. P. Vysotskiy, O. Weingart, F. Zapata and R. Lindh, *J. Comput. Chem.*, 2016, **37**, 506–541.
3. B. O. Roos, R. Lindh, P.-Å. Malmqvist, V. Veryazov and P.-O. Widmark, *J. Phys. Chem. A*, 2004, **108**, 2851–2858.
4. C. A. Goodwin, F. Ortu, D. Reta, N. F. Chilton, D. P. Mills, *Nature*, 2017, **548**, 439-442;
5. P. A. Malmqvist, B. O. Roos, B. Schimmelpfennig. *Chem. Phys. Lett*., 2002, **357**, 230−240.
6. B. O. Roos, R. Lindh, P.-Å. Malmqvist, V. Veryazov and P.-O. Widmark, *Chem. Phys. Lett*., 2005, **409**, 295–299.
7. a) P. J. Stephens, F. J. Devlin, C. F. Chabalowski, M. J. J. Frisch, *Phys. Chem*. 1994, **98**, 11623−11627; b) A. D. J. Becke, *Chem. Phys*. 1993, **98**, 5648−5652; c) C. T. Lee, W. T. Yang, R. G. Parr, *Phys. Rev. B,* 1988, **37**, 785−789; d) A. D. Becke, *Phys. Rev. A,* 1988, **38**, 3098−3100.
8. T. R. Cundari, W. J. J. Stevens, *Chem. Phys*., 1993, **98**, 5555−5565.
9. M. Perfetti, F. Pointillart, O. Cador, L. Sorace and L. Ouahab, *Molecular Magnetic Materials*, Concepts and Applications, 2016, pp. 345–368.